Sensors & Actuators: A. Physical 366 (2024) 115017

Contents lists available at ScienceDirect

Sensors and Actuators: A. Physical

journal homepage: www.journals.elsevier.com/sensors-and-actuators-a-physical

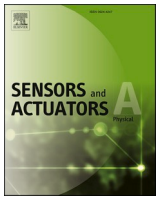

Energy harvesting using magnetostrictive materials: Effects of material anisotropy and stress multiaxiality

Yuanyuan Liu [a,b,c], Laurent Daniel [d,e], Gael Sebald [c], Mickaël Lallart [b], Kanjuro Makihara [a], Benjamin Ducharne [b,c,*]

[a] Department of Aerospace Engineering, Tohoku University, Sendai, Japan
[b] Univ. Lyon, INSA Lyon, LGEF EA682 Villeurbanne, France
[c] ELyTMaX IRL3757, CNRS, Univ Lyon, INSA Lyon, Centrale Lyon, Université Claude Bernard Lyon 1, Tohoku University, Sendai Japan
[d] Université Paris-Saclay, CentraleSupélec, CNRS, Laboratoire de Génie Electrique et Electronique de Paris, 91192 Gif-sur-Yvette, France
[e] Sorbonne Université, CNRS, Laboratoire de Génie Electrique et Electronique de Paris, 75252, Paris, France

ARTICLE INFO

Keywords:
Magnetostriction
Multiaxial stress
Behavioral anisotropy
Energy harvesting
GO FeSi

ABSTRACT

Low-frequency vibrations are common as background noise in urban and industrial environments. They originate from natural or artificial sources: road vehicles, industrial machinery, wind, etc., and constitute a ubiquitous energy source. In the framework of energy harvesting, magnetostrictive materials are an attractive alternative solution to the brittleness and geometrical limitations of piezoelectric materials. While numerous previous works dealt with uniaxial stress on selected materials, the exploration of the effects of multiaxial loadings and material anisotropy has not yet been investigated as a way to improve the performance of low-frequency vibration energy harvesting systems. In this work, we investigated the capability of grain-oriented electrical steel in an energy-harvesting context. This material has been selected as a model material, notably as it is abundant and cost-effective. It shows limited magnetostriction but significant elastic, magnetic, and magnetostrictive anisotropy. We combined experimental and predictive simulation results to discuss the possibility of increasing the levels of harvested energy by playing with the orientation of magnetic and mechanical stimuli. Various orientations of magnetic field and mechanical stress were considered with regard to the rolling direction of the material. Unexpectedly high energy density amounts, up to 10 $mJ{\cdot}cm^{-3}$, were obtained, competing with giant magnetostrictive materials like Terfenol-D or Galfenol.

1. Introduction

With the fast development of low-power electronics and the Internet of Things, wireless sensors and sensor networks are experiencing tremendous growth. Most of these devices rely on batteries characterized by a limited lifespan (e.g., due to self-discharge) and non-sustainable composition. Manufacturers are looking for alternative solutions, but the number of feasible replacement options is limited. Energy harvesting systems are a promising solution, attracting the increasing attention of the academic and industrial communities [1–4].

A complete energy harvesting system includes three main parts: an active material, a structure (mechanical, thermal, etc.), and an electrical interface [5,6]. Regarding the conversion material, magnetostrictive or piezoelectric materials can be equally used for converting energy from vibrational sources. In contrast, photovoltaic cells are limited to solar sources, and thermoelectric modules to thermal ones. Low-frequency vibrations are common background noise in urban and industrial environments, meeting the needs of self-powered sensing in such areas. They originate from many artificial and natural sources: road vehicles, industrial machinery, wind, air-conditioning units, etc., and constitute a ubiquitous energy source of high-power density [7–10].

Most existing vibrational energy harvesters rely on piezoelectric, magneto-dynamic, or magnetostrictive coupling. Piezoelectric materials are brittle, have high impedances, and lack design flexibility [11,12]. Magneto-dynamic systems are delicate to use in the low-frequency range and need substantial space. Thus, in this study, we opted for magnetostrictive conversion.

Magnetostriction is the change of shape of a magnetic specimen subjected to a magnetic field [13–18]. The converse effect (magnetization variation due to a mechanical stimulus) is called the Villari effect.

* Corresponding author at: Univ. Lyon, INSA Lyon, LGEF EA682 Villeurbanne, France.
E-mail address: benjamin.ducharne@insa-lyon.fr (B. Ducharne).

https://doi.org/10.1016/j.sna.2024.115017
Received 1 October 2023; Received in revised form 18 December 2023; Accepted 6 January 2024
Available online 13 January 2024

All energy harvesting systems based on magnetostriction exploit the Villari effect [19–22]. They convert the variation of the mechanical excitation due to natural vibrations into a change of magnetization state and, thus, magnetic flux density, which induces a voltage when associated with a dedicated electrical interface. The magnetization process is strongly anisotropic (direction-dependent), and so is magnetostriction [23–29]. From the energy harvesting point of view, magnetostrictive anisotropy means that the coupling property can be maximized according to the direction and orientation of both magnetic and mechanical excitations. Still, to our knowledge, this potentiality has never been exploited. Therefore, this work investigates the performances of Grain-oriented electrical steel (GO FeSi) in an energy harvesting context.

GO steel shows a limited magnetostriction. But it is highly anisotropic, and its magnetic behavior is well documented. Also, efficient simulation tools are available to describe its magneto-mechanical behavior [30–32]. Furthermore, its cost-effectiveness is consistent with the economic constraints of low-power sensing solutions in the framework of battery replacement. This study combines experimental and predictive simulation results to exploit the energy harvesting capability of GO FeSi. We discuss the possibility of increasing the amount of harvested energy by playing with the orientation of both magnetic and mechanical stimuli.

The manuscript is organized as follows. Section II is dedicated to the experimental methods, including the description of the so-called Ericsson cycle (in the context of the magnetostrictive energy harvesting), the experimental setup, and the tested specimens. The third section describes the simulation method. The fourth section provides discussions on simulations and experimental results. The last section includes a general conclusion and perspectives.

2. Experimental methods

A dedicated experimental process was designed to assess the influence of anisotropy on the amount of harvested energy after a complete conversion cycle. The first sub-section of this practical description defines the Ericsson cycle, which was run for energy conversion. Then, the magneto-mechanical characterization setup is detailed, followed by a complete description of the specimens and their preparation.

2.1. Ericsson cycle

At low frequencies, an energy harvesting system has to go through a complete cycle to be effective. Amongst a limited number of options, the so-called Ericsson cycle (Fig. 1), which in the context of a magnetostrictive energy harvester consists of two steps under constant stress and two under constant magnetic excitation [33–35], provides a solid basis for analysis for comparison purposes. Let us consider a magnetostrictive specimen in an unknown magnetic state bearing the effect of a mechanical tensile stress stimulus. The related magnetostrictive Ericsson cycle includes four steps:

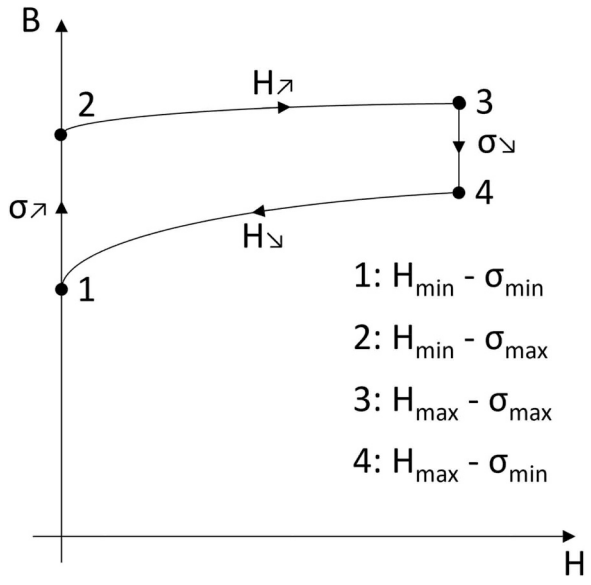

Fig. 1. B(H) magnetostrictive Ericsson cycle.

1–2: The stress stimulus starts, going from a low-stress state σ_{min} to a maximal stress value $\sigma_{max,}$ while the magnetic excitation is kept null. If the initial magnetization state is non-zero, magnetization increases under the sole effect of mechanical stress (for a positive magnetostriction material).

2–3: The stress is kept constant at σ_{max} while the magnetic excitation increases to a maximal magnetic excitation value H_{max}.

3–4: The stress decreases to the original minimal value of $\sigma_{min,}$ while the magnetic excitation is maintained at H_{max}. During this stage, the magnetization falls under the sole effect of mechanical stress.

4–1: The stress stimulus is in the low state value σ_{min}, and the magnetic excitation decreases to zero, its initial value.

The resulting closed-loop area (1–2-3–4 in Fig. 1) in the B(H) diagram (with B the magnetic flux density) is equivalent to the energy converted from mechanical to magnetic energy, which can be further converted into electrical energy. Note that such a conversion is solely done through a solid-state phenomenon (inverse magnetostriction), contrary to magneto-dynamic devices that use geometric effects.

Ericsson cycles are used to assess the energy density that can be converted from mechanical to magnetic energy. While its practical implementation is outside the scope of this study, it is considered a measure of the ultimate energy conversion capability within a material. It may serve as a comparison basis between materials and to study the effect of the orientation of magnetic field and mechanical stress.

2.2. Magneto-mechanical characterization setup

A dedicated test bench was designed to evaluate the magnetic flux density B when applying an excitation magnetic field H and uniaxial mechanical stress σ (tension and compression). Since H and σ were fully controlled, Ericsson cycles could also be measured. A descriptive picture of this experimental setup in compressive stress configuration is depicted in the top part of Fig. 2. The tensile stress configuration is shown at the bottom of the same figure.

The magnetization circuit comprised two electrical steel yokes and two $N = 55$-turns excitation coils connected in series. Each coil is wrapping a yoke, as shown in Fig. 2. The excitation coils were supplied by a Yokogawa® 7058 power amplifier (Tokyo, Japan) driven by a 33210A Agilent® (Santa Clara, California, USA) arbitrary waveform generator. A 5 Ω resistor was plugged in series with the excitation coils to monitor the electrical current. Once measured, this current was used to indirectly return the magnetic excitation field, considering that the magnetic reluctances of the yokes are negligible compared to that of the sample and according to Eq. 1:

$$H_{surf}(t) = \frac{2N \cdot I(t)}{L_e} \quad (1)$$

with $L_e = 27$ mm is the length of the specimen in the tested area. This indirect method is imperfect as some assumptions are not always fulfilled, but results still give correct orders of magnitude, i.e., consistent with the expectations and the literature. Another solution consists of local measurements using a hall probe at different heights and extrapolating the value at the surface [36,37], but this solution was discarded for space limitations. N and R were set to reach the targeted maximum magnetic field (3 $kA \cdot m^{-1}$) with a limited current and ensure a minimum inductive contribution compared to the resistive one. This condition was mandatory to control the current waveform and the magnetic field

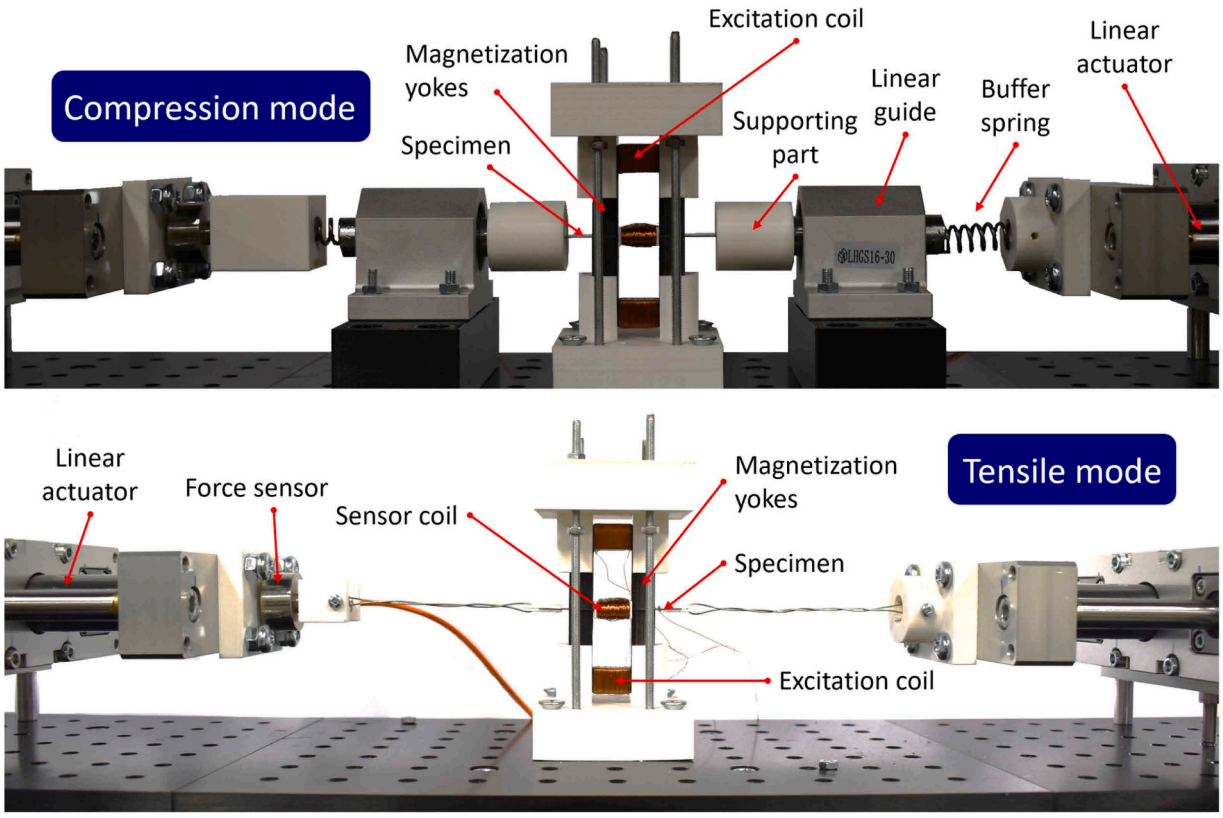

Fig. 2. Experimental setup, compression configuration (top part), and tensile configuration (bottom part).

accurately.

A n = 500-turns sensor coil was also wrapped around the tested specimens to measure the induced electromagnetic force ∅ giving the magnetic flux density:

$$B_a(t) = \frac{1}{n \cdot S} \int \varnothing(t) dt \quad (2)$$

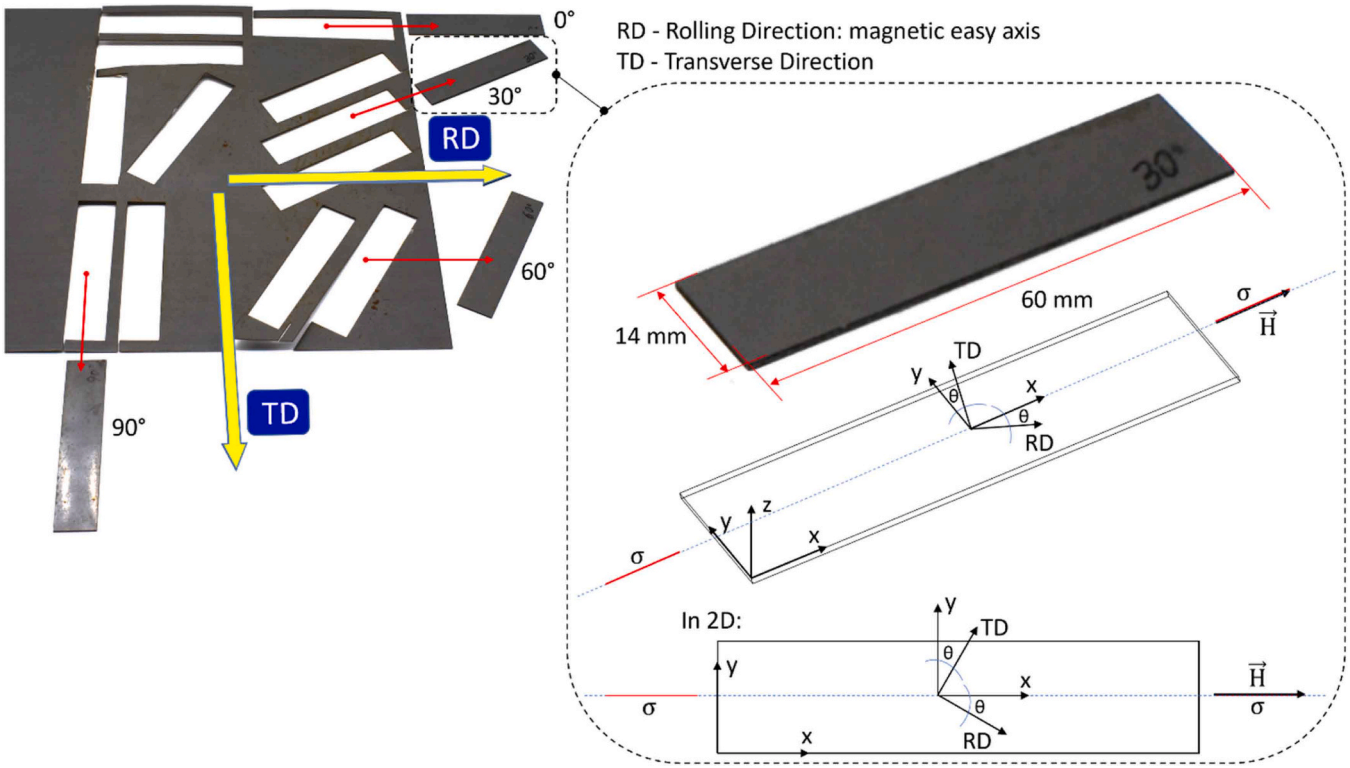

Fig. 3. Studied specimens' orientation and dimensions. Schematic of the sample, introducing material (RD, TD, **z**) and sample (**x**, **y**, **z**) coordinate systems.

where $S = 4.2\,mm^2$ (in tensile mode) and $8.4\,mm^2$ (in compressive mode) is the tested specimen cross-section.

For the mechanical stress, two Misumi® (Tokyo, Japan) RSDG306 linear actuators driven by Misumi EXRS-C1 controllers and Matlab® were used. In the compression configuration, buffer springs and linear guides were used on both sides of the tested specimen to ensure the correct application of the mechanical force. The perfect alignment of the tested specimen, the springs, and the linear actuators was obtained using two linear guides constituted of four parts:

_ an alignment spacer (in black in Figs. 2), 3D printed for an adjusted height,

_ a Misumi® LHGS 16–30 linear guide screwed on the top of the alignment spacer,

_ a Ø = 16 mm steel rod,

_ a 3 cm wide, 3D printed rod spacer (in white in Fig. 2) to avoid any magnetic interaction between the steel rod and the tested specimen.

The critical buckling load can be derived from Eqs. 3 and 4, where I* is the moment of inertia:

$$I^* = \frac{bh^3}{12} \tag{3}$$

$$F_{max} = \frac{\pi^2 E I^*}{(KL_e)^2} \tag{4}$$

b and h are the specimen's thickness and height, respectively. The parameter E denotes the specimen Young's modulus. Since the specimen is clamped vertically by the yokes, both ends of the specimen are assumed to be rotationally fixed. Consequently, the effective length factor for rotationally fixed ends, K, is 0.5. L_e represents the length of the specimen within the tested area. The critical buckling load is calculated to be 820 N, corresponding to a compressive stress level of 97 MPa, which remains below the tested specimen yield strength (285 MPa, see Table 1 below). Therefore, this study limited the maximum compressive force to 300 N to prevent buckling risk. We neglected the influence of the glue layer as its thickness was minimal compared to the other layers. Finally, all the signals were recorded with a Dewesoft® (Trbovlje, Slovenia) Sirius data acquisition card.

2.3. Experimental specimen description

The tested material was grain-oriented electrical steel (GO FeSi 3%) referenced 30JG130 from JFE steel (Tokyo, Japan) [38]. The magnetic and mechanical properties of this electrical steel grade, provided by the manufacturer, are listed in Table 1.

"A 290 × 150 mm^2 GO FeSi coated plate of easy magnetization (L/RD axis) along the plate length was cut to provide specimens with different angles with respect to RD (Fig. 3). The cutting process was electro erosion (Electric Discharge Machining, EDM), considered as the less harmful cutting method in terms of induced residual stress.

Three specimens for each investigated angle (0, 30, 60, and 90°) were prepared. Fig. 3 provides the orientation and dimensions of the studied specimens. Tension tests were done in the elastic range to avoid residual strain. Then, two specimens were glued with a Misumi (Tokyo, Japan) modified acrylic resin AY123 for each angle category to form two-layer stacks, bulk enough to bear up to 300 N compressive force. The glue contributed to the increased stiffness and load distribution of the resulting two-layer stack structure, making it less susceptible to buckling due to reduced slenderness. The exact thickness of the glue was unknown but small enough to avoid impact on the magnetostrictive response of the resulting two-layer stack. The third specimen was left untreated for possible additional reproducibility tests.

3. Simulation method

3.1. Anhysteretic behavior: the MultiScale Model (MSM)

MSM [39,40] has been built to predict the anhysteretic magneto-elastic behavior of a ferromagnetic specimen. It relies on a statistical description of the distribution of ferromagnetic domains. MSM provides tensorial information, and the anisotropy effects are naturally taken into account. The approach has been successfully applied to describe the behavior of GO steels [31,41]. The polycrystalline ferromagnetic specimen is described as an aggregate of single crystals (grains). In the multiscale model, a grain is treated as a single crystal inside the polycrystal. Each grain is supposed to be divided into a finite number of magnetic domain families. About 10^4 families for each grain orientation have been considered for the GO FeSi studied in this work. Each domain family is characterized by the orientation $\boldsymbol{\alpha}$ of the magnetization and by its potential energy W_α (Eq. 5), where W_α^k, W_α^H, W_α^σ, and W_α^{conf} stand for the magneto-crystalline (Eq. 6), magnetostatic (Eq. 7), magneto-elastic (Eq. 8), and initial configuration energy, respectively:

$$W_\alpha = W_\alpha^K + W_\alpha^H + W_\alpha^\sigma + W_\alpha^{conf} \tag{5}$$

$$W_\alpha^K = K_1\left(\gamma_1^2\gamma_2^2 + \gamma_2^2\gamma_3^2 + \gamma_3^2\gamma_1^2\right) + K_2\gamma_1^2\gamma_2^2\gamma_3^2 \tag{6}$$

$$W_\alpha^H = -\mu_0 \mathbf{H}_\alpha.\mathbf{M}_\alpha \tag{7}$$

$$W_\alpha^\sigma = -\boldsymbol{\sigma}_\alpha : \boldsymbol{\varepsilon}_\alpha^\mu \tag{8}$$

$\mathbf{H}_\alpha$, $\mathbf{M}_\alpha$, $\boldsymbol{\sigma}_\alpha$ and $\boldsymbol{\varepsilon}_\alpha^\mu$ are the magnetic field, the magnetization, the stress tensor, and the magnetostriction strain tensor defined at the magnetic domain scale, respectively. $\mathbf{M}_\alpha$ is defined by its norm (the material saturation magnetization M_s), and its direction is given by its direction cosines $\gamma_1, \gamma_2, \gamma_3$. $\boldsymbol{\varepsilon}_\alpha^\mu$ is defined by the magnetostriction constants λ_{100} and λ_{111}. K_1 and K_2 are the magneto-crystalline energy constants. The configuration term was not used (set to zero) in this study. The volume fraction f_α of a domain family is calculated from the knowledge of the potential energy of all domain families:

$$f_\alpha = \frac{\exp\left(-A_S W_\alpha\right)}{\sum_\alpha \exp\left(-A_S W_\alpha\right)} \tag{9}$$

where A_S is a material parameter that can be adjusted using the initial macroscopic susceptibility χ^0 of the unstressed anhysteretic magneti-

Table 1
30JG130 electrical steel magnetic and mechanical properties as provided by the manufacturer ("L" and "C" means the specimens cut parallel and transverse to the Rolling Direction (RD), respectively).

Grade	Thickness (mm)	Assumed density (kg/dm³)	Resistivity (μΩ·cm)	Max. Core Loss at 1.7 T (W·kg⁻¹)		Min. Magnetic Polarization at 800 A·m⁻¹ (T)	Min. Lamination Factor (%)
				50 Hz	60 Hz		
30JG130	0.3	7.65	46	1.3	1.72	1.8	95.5

Yield point (N·mm²)		Tensile strength (N·mm²)		Elongation (%)		Hardness HV (1)	Number of Bends		Lamination Factor (%)
L	C	L	C	L	C	L	C		
285	297	313	362	11	35	188	20	14	98

zation curve (Eq. 22 in [39]).

Once f_α is calculated for all magnetic domains families, the magneto-elastic response at the grain scale (magnetization $\mathbf{M}_g$ and magneto-striction strain tensor $\boldsymbol{\varepsilon}_g^\mu$) is calculated according to Eqs. 10 and 11.

$$\boldsymbol{\varepsilon}_g^\mu = \langle \boldsymbol{\varepsilon}_\alpha^\mu \rangle = \sum_\alpha f_\alpha \boldsymbol{\varepsilon}_\alpha^\mu \tag{10}$$

$$\mathbf{M}_g = \langle \mathbf{M}_\alpha \rangle = \sum_\alpha f_\alpha \mathbf{M}_\alpha \tag{11}$$

An orientation distribution function (crystallographic orientations) obtained from X-ray diffraction or Electron Back Scattering Diffraction (EBSD) measurements can be used to describe the crystallographic texture and return the behavior at the polycrystalline scale [41].

For the sake of simplicity, magnetic excitation **H** and mechanical stress **σ** are supposed to be uniform within the material. Each magnetic domain family's potential energy and volume fraction is calculated first. Then the magnetization of each grain is obtained from Eq. 11. Eventually, an average over the whole volume is performed to obtain the entire specimen magnetization **M** (volume average of the grains' magnetization):

$$\mathbf{M} = \langle \mathbf{M}_g \rangle = \int_V \mathbf{M}_g dV \tag{12}$$

This process allows constructing the stress-dependent anhysteretic magnetization curves based on a limited number of intrinsic material parameters. The magnetic flux density **B** is finally easily deduced from the magnetization using Eq. 13:

$$\mathbf{B} = \mu_0(\mathbf{H} + \mathbf{M}) \tag{13}$$

3.2. Modeling results

In this study, the simulation parameters and the crystallographic texture data for a typical GO FeSi were taken from [41] (Hi-B, 300 μm thick from Nippon Steel, Tokyo, Japan).

The crystallographic texture of GO electrical steel is strong, so a limited number of orientations (60 here) is sufficient to obtain accurate simulation results. The simulation parameters are summarized in Table 2. Fig. 4 illustrates MSM predictions. Fig. 4.a shows simulated anhysteretic curves for the GO FeSi along different orientations in the lamination plane in the stress-free state. All along the paper, the angle θ indicates the angle between the magnetic field ($\mathbf{H}_{surf} = H\mathbf{x}$) and the rolling direction (RD, see Fig. 3). Therefore, $\theta = 0$ indicates a magnetic field applied along the Rolling Direction (RD - easy axis), $\theta = 90°$ along the transverse direction (TD).

Fig. 4.b gives the induction levels for a given H as a function of θ. The significant differences between RD and TD are noteworthy, and an especially unfavorable direction is observed at approximately 55° (usual observation for GO electrical steel [31,41]). Interestingly, the contrast between low and high magnetic field response is more significant for angles greater than 60°. Fig. 4.c compares simulated anhysteretic curves and experimental reconstructed ones obtained by averaging, for a given magnetic excitation, measured cycles' increasing and decreasing branches without stress.

Table 2
Simulation parameters for the GO FeSi [31].

Quantity	M_S	K_1; K_2	λ_{100} ; λ_{111}	A_S	C_{1111} ; C_{1122} ; C_{1212}
Unit	$A{\cdot}m^{-1}$	$kJ{\cdot}m^{-3}$	-	$m^3{\cdot}J^{-1}$	GPa
Value	$1.37{\cdot}10^6$	38; 0	$23{\cdot}10^{-6}$; $-4.5{\cdot}10^{-6}$	$2{\cdot}10^{-2}$	202; 122; 115

3.3. From the MSM anhysteretic prediction to the Ericsson energy harvesting cycle

The MSM, as implemented here, is anhysteretic. Hysteresis losses are not taken into account. However, the coercive field in GO FeSi at low frequency is small, and the studied Ericsson cycles do not generate significant magnetic hysteresis. This issue has already been discussed in the case of ferroelectric materials [42]. The calculation of the harvested energy from the anhysteretic curves is illustrated in Fig. 5 and yields:

$$\text{Ericsson cycle } energy = \int_0^{H_{max}} B_{anh\_\sigma_{max}}\, dH - \int_0^{H_{max}} B_{anh\_\sigma_{min}}\, dH \tag{14}$$

where H_{max} is the maximal value of H, σ_{max} is the stress value in the 1 - 3 branch (Fig. 5), and σ_{min} in the 4 - 2 branch.

Even if all energy harvesters are intrinsically dynamic, the MSM predictions are static (frequency-independent), so their range of validity is restricted to low frequency mechanical source.

4. Exploitation of experimental and simulation methods in a magnetostrictive energy harvester context

The experimental setup described in Section II was limited to configurations where the stress and the magnetic field axis are parallel. Regarding MSM, predictions can be obtained for any excitation configuration. To assess the influence of anisotropy and multiaxiality of stress on the amount of energy harvested through Ericsson cycles, we opted for the following methodology:

- MSM predictions were validated using experimental configurations where data are available (uniaxial stress σ, and $\mathbf{H}_{surf}$ on the same axis).
- Additional numerical computations were performed in various configurations to identify the most appropriate one for maximizing the converted energy.

4.1. First case study: magnetic excitation Hsurf and uniaxial mechanical stress σ in the same direction

Fig. 6.a depicts the first series of simulation results. Magnetic excitation ($\mathbf{H}_{surf} = H\mathbf{x}$) and mechanical stress ($\boldsymbol{\sigma} = \sigma\mathbf{x} \otimes \mathbf{x}$) were imposed along the length of the sample. Tests were done from $\theta = 0$ to 90° with a $\Delta\theta = 1°$ angle step (0° corresponds to RD). The magnetic excitation amplitude was 3 $kA{\cdot}m^{-1}$. The mechanical stress was compressive along **x** and varied from −10 to −100 MPa. Results confirm the very strong anisotropy of the material. Simulations under tensile stress were also run for the same range of stress amplitudes but not plotted here for conciseness (as results showed less relevance in the targeted applicative framework). Fig. 6.b and 6.c show comparisons between experimental and modelling results for compressive and tensile stresses in the 0 - 25 MPa range for which experimental tests were performed. Measurements and predictions show similar order of magnitude for the harvested energy. Tension configurations provide much lower harvested energy levels compared to compression configurations. The measurement uncertainty is, therefore, also larger in tension. Under compression, larger amounts of converted energy were obtained at $\theta = 0°$. Oppositely $\theta = 55°$, known as the worst angle for magnetization, gave the lowest quantity of energy harvested. The Transverse Direction (TD) provides higher converted energy than other directions in tensile stress configuration. Such trends are also observed for numerical results. Fig. 7 shows simulations and measurements for the Ericsson cycle energy vs. the magnetic field excitation amplitude for different compressive stress levels and angles.

A discrepancy can be observed in the comparison between the experimental and the simulation results of Fig. 6.c for θ lower than 30°. Tensile stress has a magnetic softening effect. When $\theta < 30°$, GO FeSi is already highly magnetically soft. Therefore, the influence of tensile stress is expected to be very limited. In such conditions where the effect

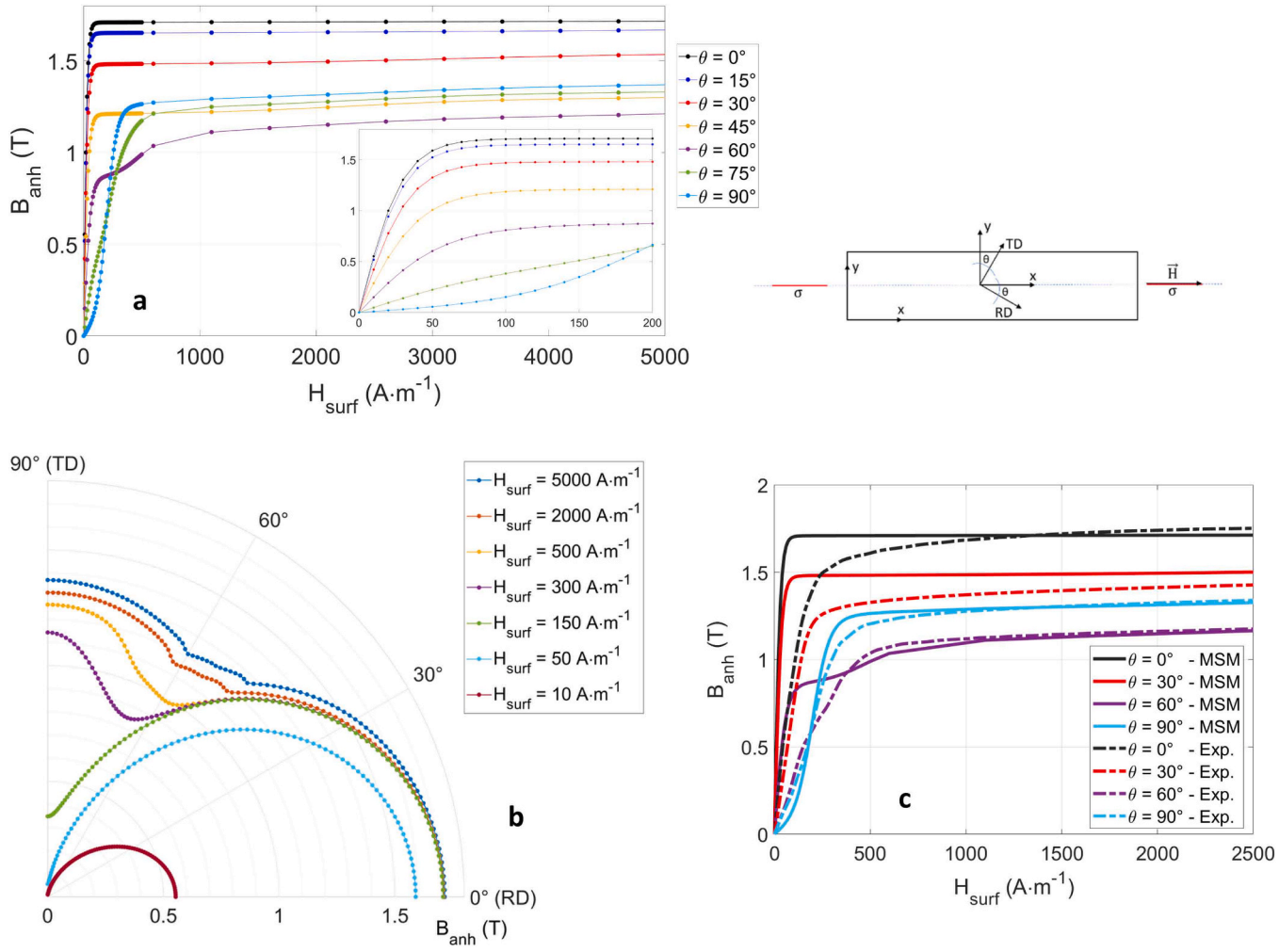

Fig. 4. **a** Simulated anhysteretic curves for different orientations in the lamination plane. **4.b** Induction level for a given H as a function of θ. **4.c** Comparison simulation/measurement for the anhysteretic behaviors.

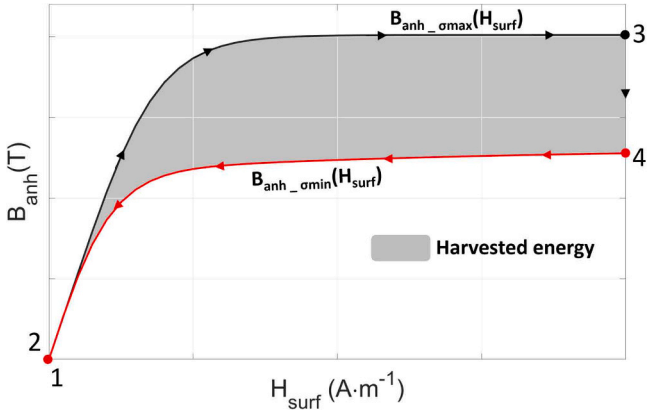

Fig. 5. Definition of the Ericsson cycle energy from the anhysteretic curves.

of stress is shallow, the accuracy of MSM is limited. Fig. 6.c experimental results were unexpected but can be attributed to the limitations of the testing equipment. The most reliable explanation can be found in the shallow level of permeability at saturation, favoring the magnetic leakages and reducing the overall accuracy of the characterization bench. A discrepancy can also be observed in the comparisons of Fig. 7, especially under the compressive stress of −10 MPa. In this range of stress, the impact on the anhysteretic behavior is limited, as well as the simulation accuracy.

Finally, Fig. 8 shows simulations and measurements of the amount of Ericsson cycle vs. the stress levels for different angles at H = 3 kA·m^{-1}. For this representation, the comparison simulations/measurements appear to be much closer. The general trends are respected such as the order vs. the angle distribution.

Both modeling and experimental results confirm the superior performance of compressive stress over tensile one. Fig. 6.a exhibits a region with a very strong orientation sensitivity (between 45 and 65°). In this region, the obtention of accurate simulation results is challenging as a slight error in the angle (both in the experimental results or the texture data definition) yields high uncertainty. Another simulation difficulty comes from the high sensitivity in the low-stress region. Conversely, high field/high-stress levels produce more stable and reliable results. The magnetic microstructure reaches a saturation state for such loadings, leading to smaller variations in the magnetic response. Consequently, MSM appears more trustable at high field and stress, away from the θ = 55° orientation. These regions will be investigated explicitly in the following.

4.2. *Second case study: magnetic excitation H_{surf}, and mechanical stress σ in different directions*

Excitation stress and magnetic field were uniaxial and along the same axis in sub-Section 2.2 experimental setups. But natural vibrations

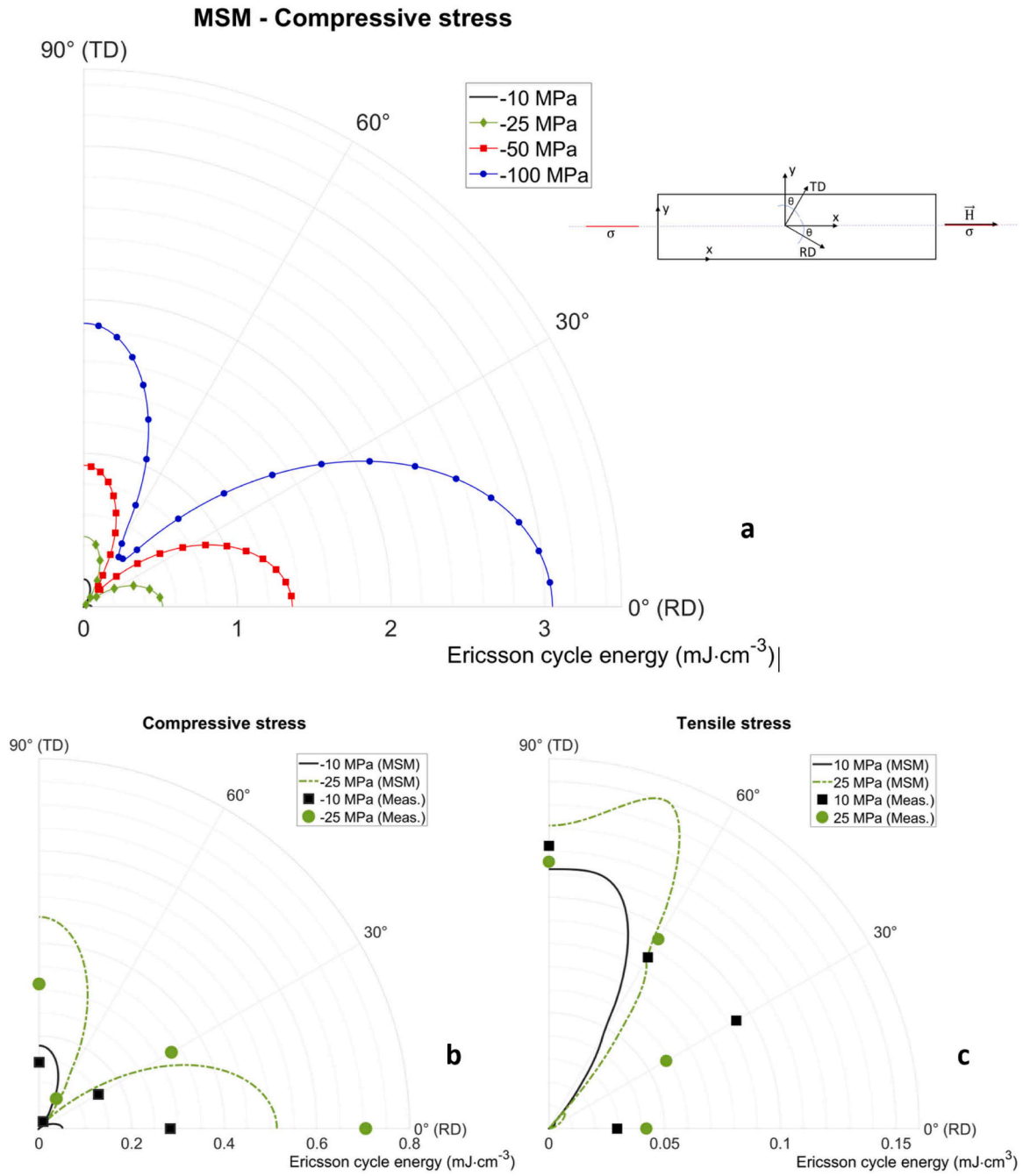

Fig. 6. Effect of the sample orientation on the harvested energy for uniaxial stress configurations ($\mathbf{H}_{surf} = H\mathbf{x}$ and $\boldsymbol{\sigma} = \sigma\mathbf{x} \otimes \mathbf{x}$), **6.a** Modelling results under compressive stress ($\sigma < 0$ and max(H)= 3 kA·m^{-1}); **6.b** Comparison between experiments and modeling for compressive configurations; **6.c** Comparison between experiments and modeling for tensile configurations.

could come multiaxially, or a structure may be designed in this objective, even if a preferential acceleration axis is usually observed. Benefits can be anticipated by considering such multiaxiality in future energy harvesting devices. MSM works with a full tensorial representation of the magnetic and mechanical quantities. It can therefore be used to predict complex configurations beyond the limitation of laboratory test benches. This subsection is limited to numerical predictions. In the first configuration, stress remains uniaxial but was applied at 90° from the magnetic field ($\mathbf{H}_{surf} = H\cdot\mathbf{x}$ and $\boldsymbol{\sigma} = \sigma\cdot\mathbf{y} \otimes \mathbf{y}$). Then, bi-axial stress was tested under different configurations ($\mathbf{H}_{surf} = H\cdot\mathbf{x}$ and $\boldsymbol{\sigma} = \sigma_{xx}\cdot\mathbf{x} \otimes \mathbf{x} + \sigma_{yy}\cdot\mathbf{y} \otimes \mathbf{y}$). It was finally followed by a tri-axial test that we anticipate as the most efficient configuration in energy harvesting ($\mathbf{H}_{surf} = H\cdot\mathbf{x}$ and $\boldsymbol{\sigma} = \sigma_{xx}\cdot\mathbf{x} \otimes \mathbf{x} + \sigma_{yy}\cdot\mathbf{y} \otimes \mathbf{y} + \sigma_{zz}\cdot\mathbf{z} \otimes \mathbf{z}$).

4.2.1. *Uniaxial stress configuration: θ varying from 0 to 90° from RD and σ at θ + 90°*

In this subsection, mechanical stress and magnetic excitation were simulated as uniaxial but with an angle difference of 90° ($\mathbf{H}_{surf} = H\cdot\mathbf{x}$ and $\boldsymbol{\sigma} = \sigma\cdot\mathbf{y} \otimes \mathbf{y}$). As in Section 4.1, simulations were done from $\theta = 0$ to 90° with a $\Delta\theta = 1°$ angle step, where $\theta = 0°$ corresponds to RD (easy magnetization axis). The magnetic excitation amplitude was 3 kA·m^{-1}, and the mechanical stress varied from $\sigma = -100$ to 100 MPa. It is worth noting the comparable maximum levels of harvested energy between Fig. 6.a and Fig. 9. Additionally, it can be observed that compressive and tensile stresses can produce a similar amount of harvested energy as long as the magnetic field is appropriately oriented with respect to the uniaxial stress. While an increase in the magnetic

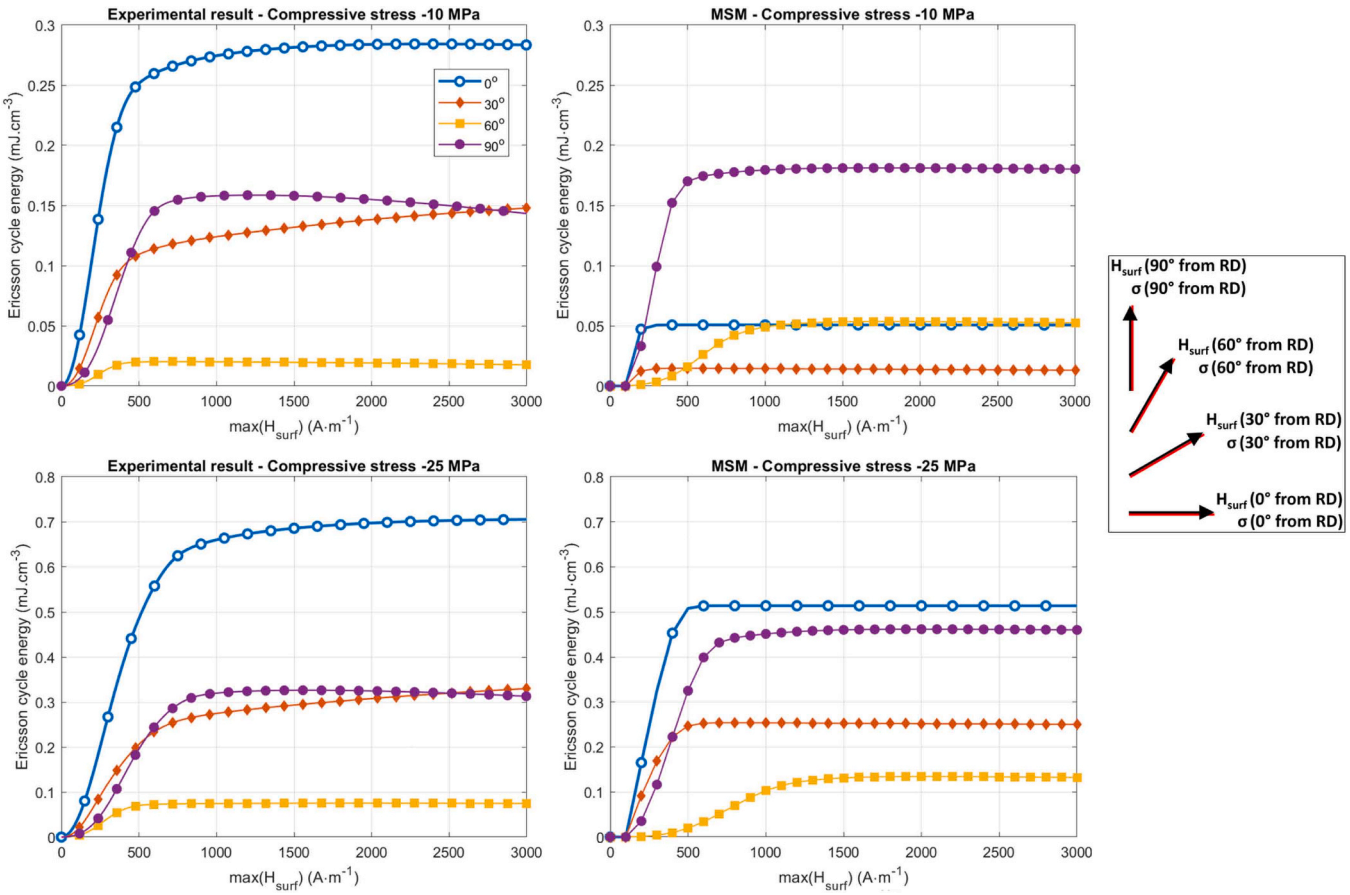

Fig. 7. Harvested energy as a function of the maximum applied magnetic field for uniaxial compressive configurations ($\mathbf{H}_{surf} = H\mathbf{x}$ and $\boldsymbol{\sigma} = \sigma\mathbf{x} \otimes \mathbf{x}$) for different sample orientations with respect to RD. Left: experimental results; right: modeling results.

field would generate the same amount of energy in the compressive case of Fig. 10.a (due to saturation), improvement can still be expected in the tensile case of Fig. 10.b.

To conclude with these uniaxial stress situations, we can claim that materials with positive magnetostriction coefficients (like the GO FeSi) will provide higher energy harvested when compression is imposed in the field axis. A tension load at 90° is another favorable configuration, yielding a very close value of converted energy.

4.2.2. Biaxial stress first configuration: σ_{uu} along RD, σ_{vv} along TD and H_{surf} at $\theta = 0°$, 30°, 60°, and 90° from RD (mechanical stress set, magnetic field rotating)

Fig. 12 depicts bi-axial stress simulations. σ_{uu} was along RD, σ_{vv} along TD (Fig. 11), and $\mathbf{H_{surf}}$ at $\theta = 0$, 30, 60, and 90° from RD (definitions in Fig. 11)(Max(H) = 3000 A·m^{-1}, $\sigma_{uu,}$ and σ_{vv} varied from − 25 to 25 MPa).

The Ericsson energy was calculated in two steps: a first simulation under the effect of the magnetic field only and a second where both stress and magnetic field are considered. Then, the Ericsson cycle energy was calculated as described in sub-Section 2.1.

The highest energy levels were obtained when $\mathbf{H_{surf}}$ was along RD or TD and when the compression and the magnetic field axis were parallel, and tensile stress was imposed on the other axis. The tensile and compressive stresses work together and produce more harvested energy. Isovalues of the elastic energy W_{el} are also shown in Fig. 12. The elastic energy shows the amount of mechanical energy available in the system. It allowed us to compare the different configurations with respect to the energy available for harvesting. The details for its calculation are given in Appendix A. It is clear from Fig. 12 that a high level of elastic energy in the structure does not guarantee a high level of harvested energy. The stress tensor's form and orientation play a significant role.

4.2.3. Biaxial stress second configuration: σ_{xx} and H_{surf} at 0°, 30°, 60°, 90° from RD, σ_{yy} at 90°, 120°, 150°, 180° from RD (mechanical stress and magnetic field rotating simultaneously)

Fig. 13 depicts bi-axial stress simulations: $\mathbf{H}_{surf} = H\cdot\mathbf{x}$ and $\boldsymbol{\sigma} = \sigma_{xx}\cdot\mathbf{x}\otimes\mathbf{x} + \sigma_{yy}\cdot\mathbf{y}\otimes\mathbf{y}$. Tests were performed for $\theta = 0°$, 30°, 60°, and 90° from RD. Again, Max(H) = 3000 A·m^{-1}, $\sigma_{xx,}$ and σ_{yy} varied from − 25 to 25 MPa. As noticed in 4.2.2, the highest energy levels are obtained when $\mathbf{H_{surf}}$ field is along RD or TD, and when compression is imposed along the magnetic field direction and tensile stress along the other axis. The system's elastic energy level has also been plotted to allow comparison. Again, it is clear that similar levels of elastic energy can lead to different levels of harvested energy depending on the form and orientation of the stress tensor.

4.2.4. Triaxial stress: towards a maximum amount of harvested energy

The underlying motivation of this work is broader than defining ideal stress and field conditions for maximizing the harvested energy. It also aims at predicting this maximum amount. For this, we considered triaxial stress conditions in the next series of simulations: $\mathbf{H}_{surf} = H\cdot\mathbf{x}$ and $\boldsymbol{\sigma} = \sigma_{xx}\cdot\mathbf{x}\otimes\mathbf{x} + \sigma_{yy}\cdot\mathbf{y}\otimes\mathbf{y} + \sigma_{zz}\cdot\mathbf{z}\otimes\mathbf{z}$. σ_{xx}, σ_{yy}, $\sigma_{zz,}$ were tested for − 100, 0, and 100 MPa.

Those values were set to ensure that the resulting local stress remains lower than the yield stress threshold. H maximal value was set to 3000 A·m^{-1} for comparison. The anisotropy influence was verified by imposing $\mathbf{H_{surf}}$ along RD first and rotating it with a 30° angle step up to 90°. The best results for each angle configuration are displayed in Fig. 14. Fig. 14 best configurations were set when maximum compression was imposed along the magnetization direction and maximum

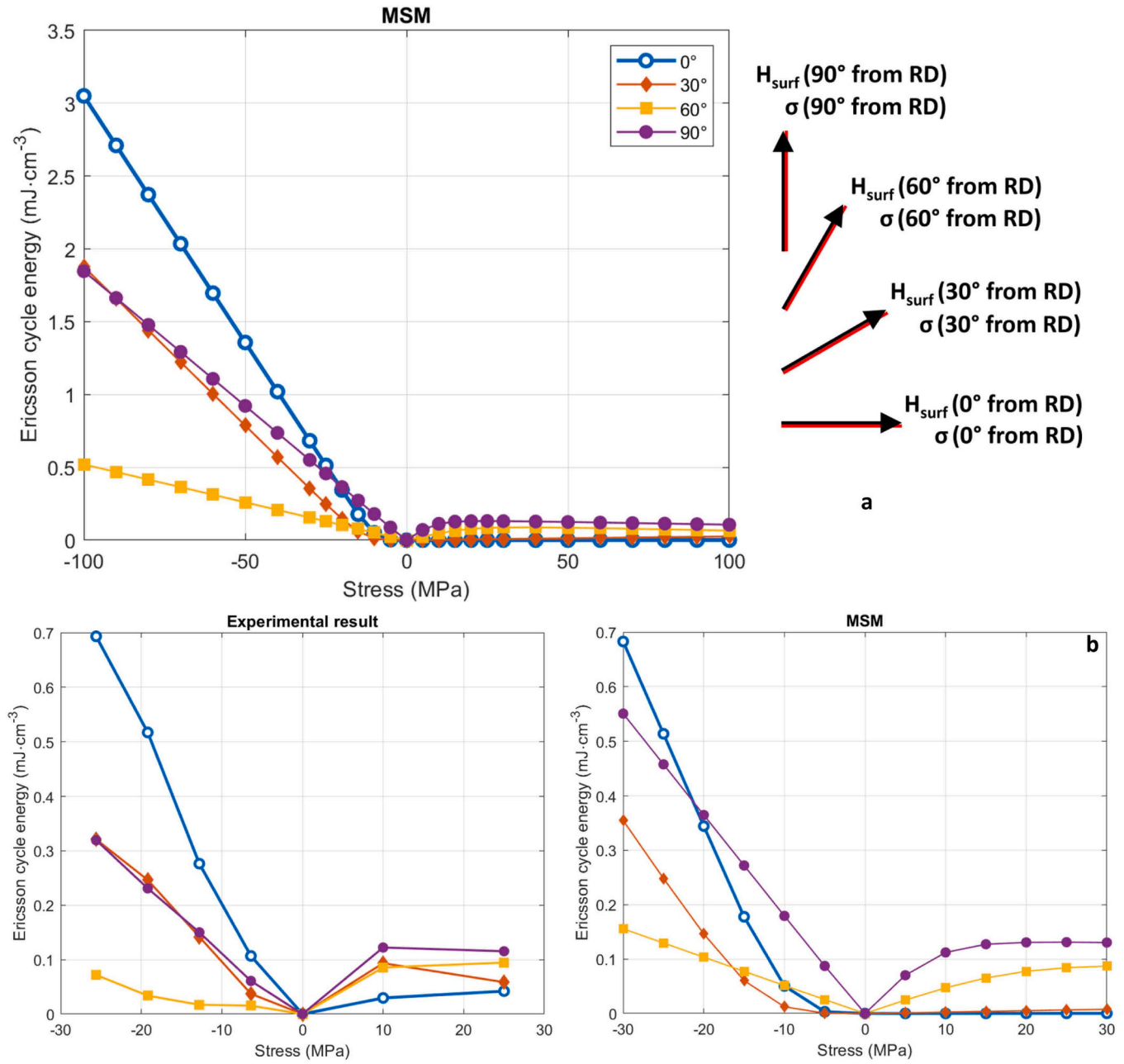

Fig. 8. Effect of the sample orientation on the harvested energy for uniaxial stress configurations ($\mathbf{H}_{surf} = H\mathbf{x}$ and $\boldsymbol{\sigma} = \sigma\mathbf{x} \otimes \mathbf{x}$): **8.a** Modelling results for max(H)= 3 kA·m^{-1}; **8.b** Comparison between experiments (left) and modeling (right).

tension along the other axes. In such a configuration, the parallel compressive and perpendicular tensile stresses effects superimpose to profoundly impact the magnetic response. A significant increase of the energy by 20% is obtained when $\mathbf{H}_{surf}$ is along RD, σ_{xx} in compression, and σ_{yy} and σ_{zz} in traction, which leads to the highest reachable energy level from the best combination of available elastic energy and magneto-mechanical conversion abilities. On the one hand, RD is the easy axis, and the zero stress anhysteretic curve is very straight and reaches full saturation with a minimum magnetic field. On the other hand, the tensile stress imposed on the y and z-axis enhanced the compressive effect and contributed to the laying down impact of the resulting anhysteretic curve. This effect can also be observed for $\mathbf{H}_{surf}$ along TD results, but the zero-stress anhysteretic curve exhibits much lower flux density leading to lower resulting energy. $|\boldsymbol{\sigma}| = 100$MPa is high for a real life application. Still, mechanical amplification methods exist (see [43] for illustration) but the cross-section of the magnetostrictive material must be low. In Fig. 14, max(H) $= 3$ kA·m^{-1} appeared to limit the maximum amount of energy. To overcome this limitation, we ran a last series of simulations where max(H) was set to 15 kA·m^{-1}. Such a high magnetic field ensured that the flux density saturation was reached for all mechanical stress configurations. For simplicity, uniaxial compressive stress configuration was considered again in these last simulations. The stress level has been tested up to −400 MPa, close to the compressive yield point but still below.

A remarkable energy density of 13.1 mJ·cm^{-3} is finally obtained under the extreme compressive stress of −400 MPa. This value shows the order of magnitude of the maximum energy level that can be harvested from an Ericsson cycle on a GO Iron-Silicon steel. Fig. 15 right-hand plot shows that in these extreme stress conditions, max(H) $= 10$ kA·m^{-1} is enough to saturate the materials and close the Ericsson loop. It would be interesting to confirm Fig. 15 experimentally. Still, for this, a new experimental setup is required, along with specimens of

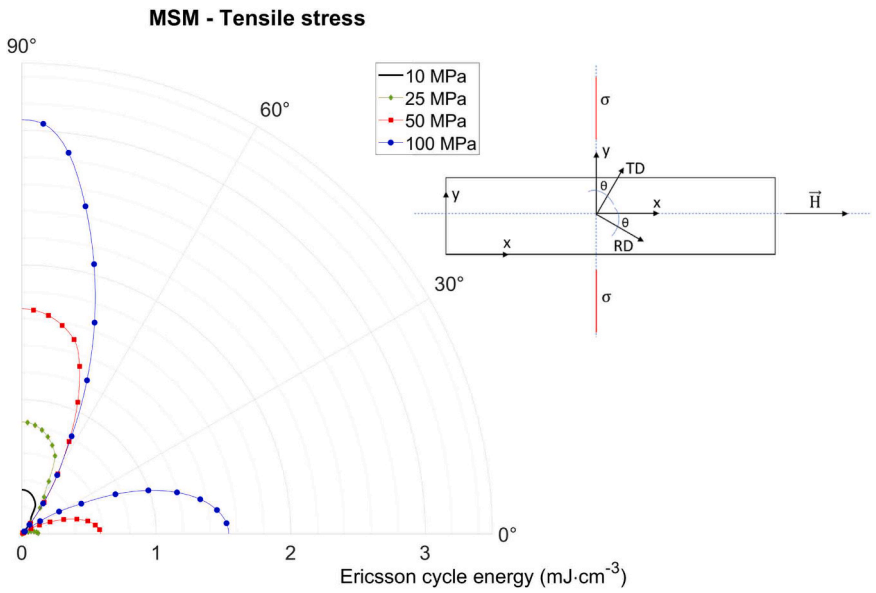

Fig. 9. Effect of the sample orientation on the harvested energy for uniaxial stress configurations with stress perpendicular to the applied magnetic field ($\mathbf{H}_{surf} = H\cdot\mathbf{x}$ and $\boldsymbol{\sigma} = \sigma\cdot\mathbf{y}\otimes\mathbf{y}$): modelling results for max(H)= 3 kA·m^{-1}.

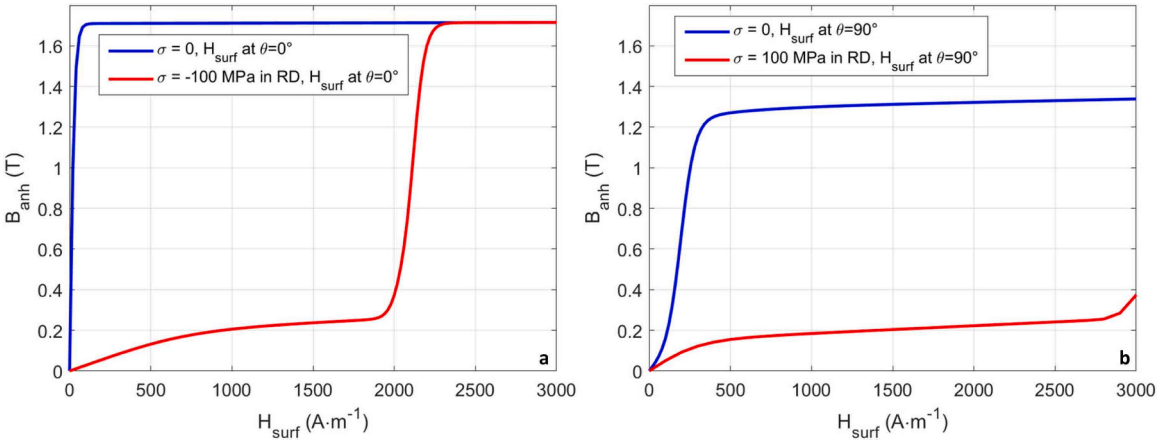

Fig. 10. Graphical illustration of the predicted Ericsson cycles with the MSM for two configurations: **10.a** $\mathbf{H}_{surf} = H\cdot\mathbf{x}$, $\boldsymbol{\sigma} = \sigma\cdot\mathbf{x}\otimes\mathbf{x}$ with $\theta = 0$ ($\mathbf{x}$ = RD); **11.b** $\mathbf{H}_{surf} = H\cdot\mathbf{x}$, $\boldsymbol{\sigma} = \sigma\cdot\mathbf{y}\otimes\mathbf{y}$ with $\theta = 90°$ ($\mathbf{x}$ = TD).

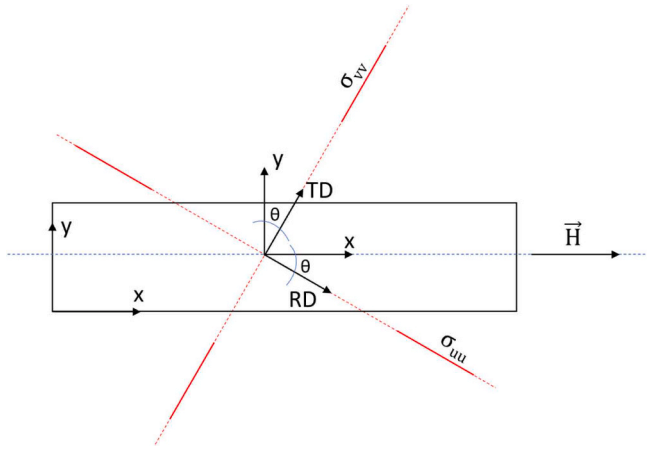

Fig. 11. 4.2.2 vectors and tensors reference.

different geometry.

4.3. Discussion

Magnetostriction is described in scientific literature as a promising way to convert a mechanical source into electrical energy and is promoted for low-frequency vibration energy harvesting. In these articles, expensive materials characterized by high magnetostrictive coefficients, like Terfenol-D or Galfenol, are always considered [44–46]. Still, in this study, we opted for a new paradigm: instead of giant uniaxial magnetostriction materials, we opted for a cheap and widespread Grain Oriented Iron-silicon steel and tried to explore the potential offered by the material anisotropy and the multiaxiality of stress. More specifically, we verified if anisotropy could be a way to improve the performance of the energy harvester and tried to determine the best stress configuration for maximizing the amount of energy harvested.

A multiscale model describing the magneto-mechanical anhysteretic behavior of the tested laminations was used to simulate precisely the Ericsson cycles. A first series of simulations was proposed in the experimental setup conditions developed for this study. The comparisons between simulations/measurements served as a basis for the model

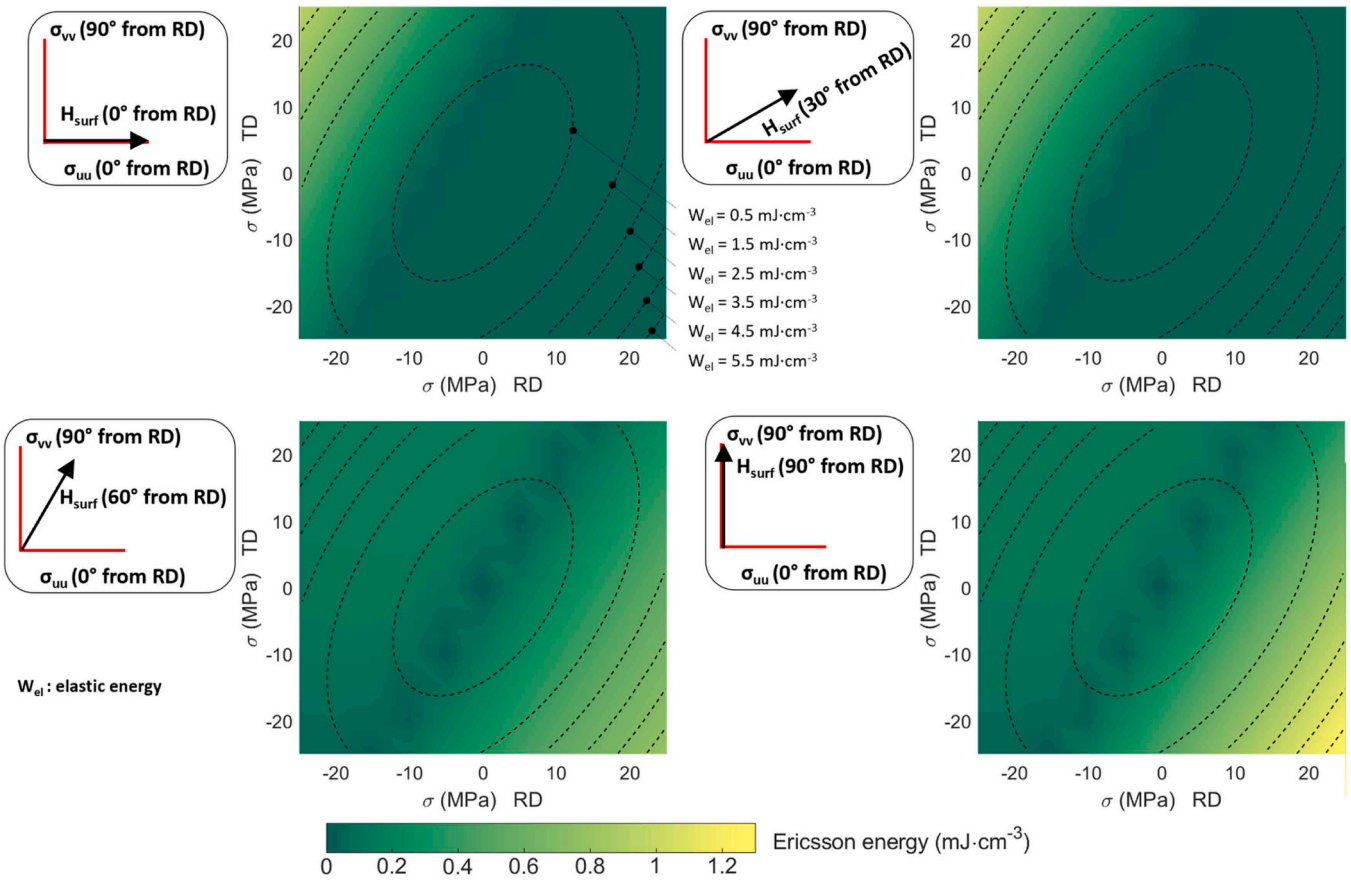

Fig. 12. Ericsson energy in 4.2.2 bi-axial configuration ($\max(H_) = 3\ \mathrm{kA{\cdot}m^{-1}}$).

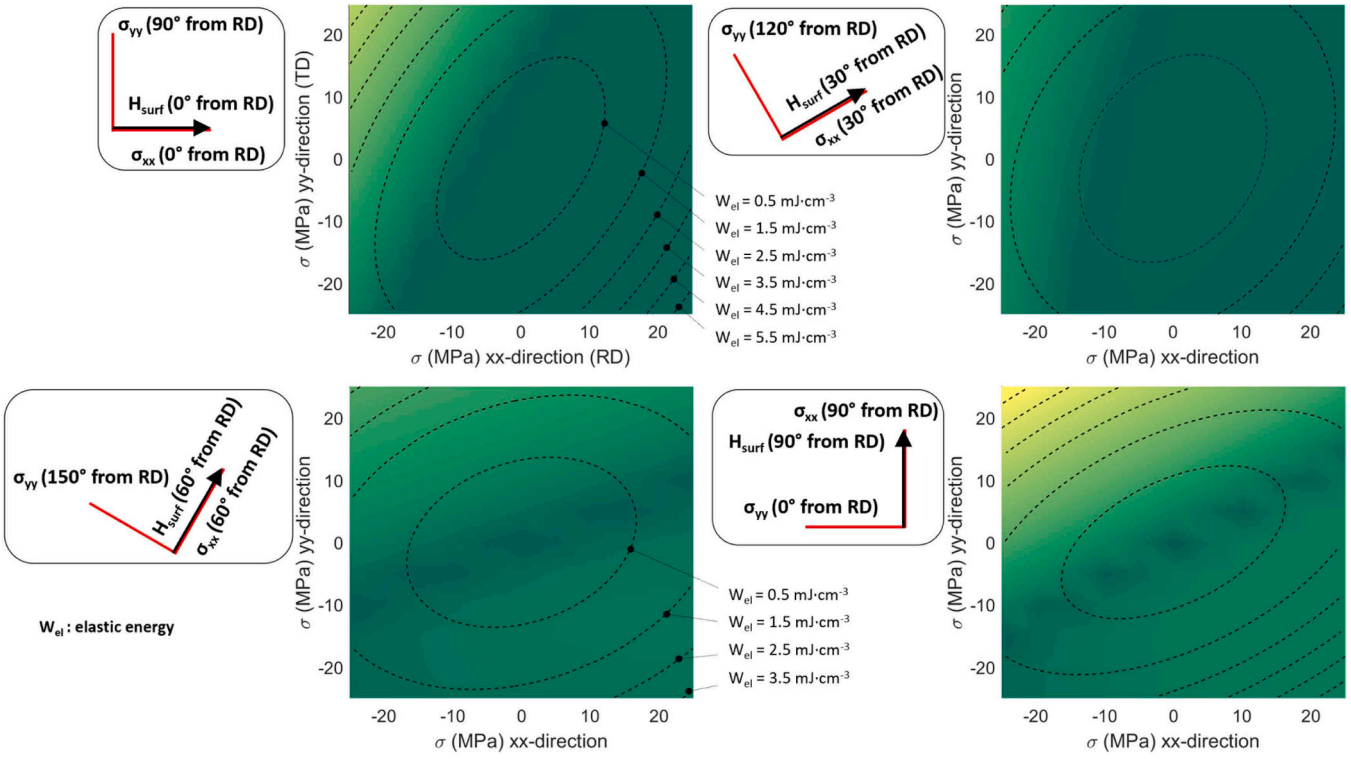

Fig. 13. Ericsson energy in 4.2.3 bi-axial configuration ($\mathbf{H}_{surf} = H{\cdot}\mathbf{x}$ and $\boldsymbol{\sigma} = \sigma_{xx}{\cdot}\mathbf{x} \otimes \mathbf{x} + \sigma_{yy}{\cdot}\mathbf{y} \otimes \mathbf{y}$) with $\max(\mathrm{H}) = 3\ \mathrm{kA{\cdot}m^{-1}}$.

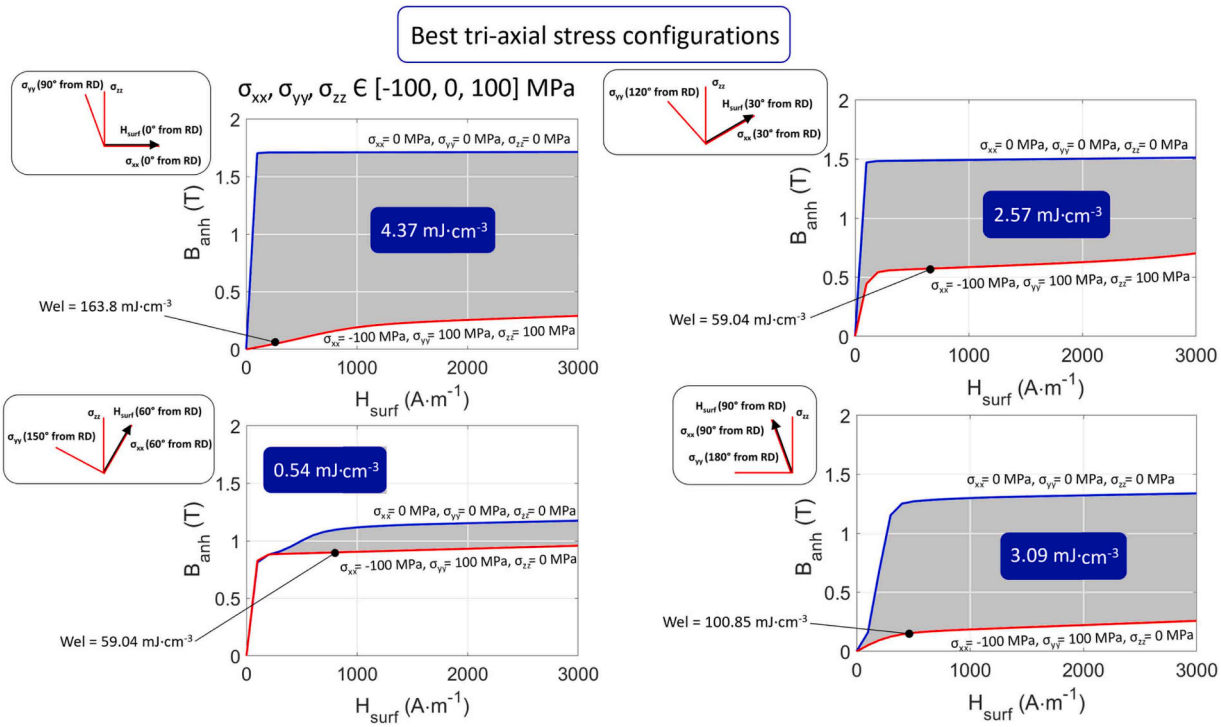

Fig. 14. Tri-axial stress, best results for each angle configuration (max(H) = 3 kA·m^{-1}).

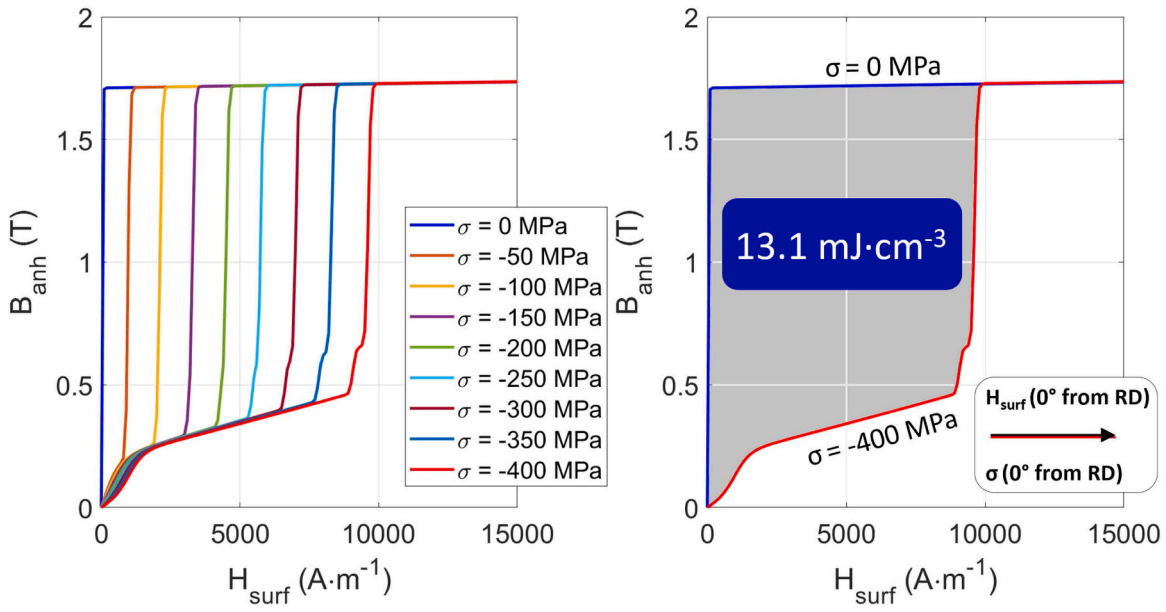

Fig. 15. Uniaxial maximal compressive stress and magnetic field along RD and the resulting energy.

validation. The model was then further used to anticipate the energy harvesting capability of the GO FeSi for configurations not accessible through the available test setup.

To allow for a simple criterion for the maximization of the harvested energy, an equivalent stress σ_{eq} was sought. This equivalent stress defines the uniaxial stress applied along RD, which provides the same amount of harvested energy as the actual stress state $\boldsymbol{\sigma}$. σ_{eq} is written in the form

$$\sigma_{eq} = \alpha\sigma_{\parallel} + \beta\sigma_{\perp} + \gamma\sigma_{sh} \tag{15}$$

where $\sigma_{\parallel}$, $\sigma_{\perp}$ and σ_{sh} are the normal component of the stress tensor along RD, the normal component of the stress tensor along TD, and the shear component of the stress tensor in the RD-TD plane, respectively. α, β, and γ incorporate the anisotropy effect. They are functions of the magnetic field orientation θ. The functions α, β and γ are illustrated in the insets of Fig. 16. α was identified from simulations under uniaxial stress applied parallel to the magnetic field (simulations for which $\sigma_{\perp}$ and σ_{sh} are zero). β was identified from simulations under biaxial stress with one principal component parallel to the magnetic field (4.2.2 configuration for which σ_{sh} is zero). γ was identified from simulations under biaxial stress with principal components along RD and TD (4.2.3 configuration). It is evident from Fig. 16 that there is a connection between the θ-dependence of α, β and γ and the magnetic anisotropy of the material reflected

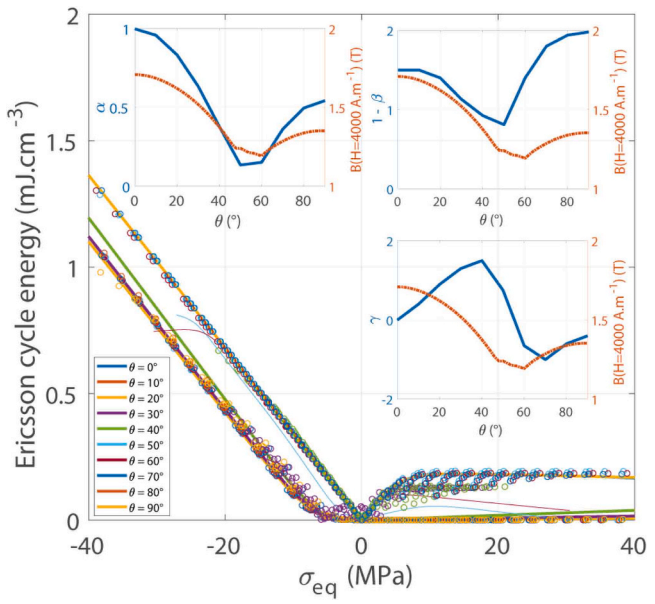

Fig. 16. Summary of all simulations performed: harvested energy as a function of the proposed equivalent stress for a maximum applied magnetic field of 4 kA.m^{-1}. The lines show the results for uniaxial configurations, while each marker corresponds to a biaxial configuration. The insets show the θ-dependence of the parameters α, β and γ used in the definition of the equivalent stress.

(in red in the insets) by the θ-dependence of the magnetic induction at 4 kA.m^{-1}.

The main plot of Fig. 16 summarizes all the simulations performed in this study for a given magnetic field amplitude (namely 4 kA·m^{-1}). The harvested energy from each Ericsson cycle is plotted as a function of the proposed equivalent stress σ_{eq}. Using this representation, the criterion to maximize the Ericsson cycle energy becomes clear: the best configuration is the configuration leading to the highest intensity of the equivalent stress in compression. Configurations with a positive σ_{eq} appear non-optimal, with low levels of harvested energy.

5. Conclusion

Finally, the conclusions of this work can be summarized as follows:

_ A multiaxial magnetoelastic model was implemented to investigate the most favorable configurations to harvest elastic energy from an Ericsson cycle. The model was validated using a dedicated uniaxial experimental setup.

_ Ericsson cycle is a non-resonant harvesting method, it requires harvesting as much energy as possible in a short time (to avoid energy dissipation). In such a case, the highest the coupling, the highest the harvested energy.

_ It was shown that compressive stress along the magnetic field direction is the most efficient way to convert elastic energy to magnetic energy using an Ericsson cycle. A tension stress superimposed along a direction perpendicular to the applied field has a constructive effect, leading to a larger amount of harvested energy.

_ The proposed modeling approach allows assessing a given magneto-elastic configuration, incorporating the effects of elastic, magnetic, and magnetostrictive anisotropy.

_ An equivalent stress was proposed, allowing a straightforward assessment of the efficiency of a given magneto-elastic configuration for energy harvesting applications.

_ For the GO FeSi used in this study, the maximum level of harvested energy during an Ericsson cycle was for a compressive stress level (400 MPa) close to the yield stress and for a magnetic field value along RD of the order of 10 kA·m^{-1}.

_ A maximum of 13.1 mJ·cm^{-3} was predicted by MSM to be the maximum level of energy potentially available for such conversion. Such an unexpectedly high amount lies in the same range as the giant magnetostrictive materials usually studied for energy harvesting applications [47].

_ A bidirectional DC-DC converter and an excitation coil are required to generate the Ericsson cycle. Real-time monitoring of input current and voltage would lead us to the amount of energy harvested.

CRediT authorship contribution statement

Ducharne Benjamin: Conceptualization, Software, Supervision, Writing – original draft. **Lallart Mickaël:** Conceptualization, Writing – review & editing. **Makihara Kanjuro:** Writing – review & editing. **Daniel Laurent:** Conceptualization, Data curation, Methodology, Software, Writing – review & editing. **Sebald Gael:** Conceptualization, Writing – review & editing. **Liu Yuanyuan:** Investigation, Writing – review & editing.

Declaration of Competing Interest

The authors declare that they have no known competing financial interests or personal relationships that could have appeared to influence the work reported in this paper.

Data Availability

Data will be made available on request.

Appendix A. Calculation of the elastic energy

W_{el} is classically defined from the double dot product of the stress with the elastic strain $\boldsymbol{\varepsilon}^e$ (Eq. A.1). The elastic strain is obtained from the stress tensor using the Hooke law (Eq. A.2), where $\boldsymbol{S}$ is the compliance tensor of the material. For the GO FeSi of this study, the macroscopic compliance tensor $\boldsymbol{S}$ was obtained from the single crystal cubic elastic coefficients (C_{11}; C_{12}; C_{44}) given in Table 2 [34] and the crystallographic texture data using a self-consistent approach [48]. The corresponding compliance tensor is given by Eq. A.3 in Voigt notation.

$$W_{el} = \frac{1}{2}\boldsymbol{\sigma} : \boldsymbol{\varepsilon}^e \tag{A.1}$$

$$\boldsymbol{\varepsilon}^e = \boldsymbol{S} : \boldsymbol{\sigma} \tag{A.2}$$

$$\boldsymbol{S} = \begin{pmatrix} 8.75 & -3.23 & -3.28 & & & \\ -3.23 & 4.96 & 0.51 & & 0 & \\ -3.28 & 0.51 & 5.01 & & & \\ & & & 24.06 & 0 & 0 \\ & 0 & & 0 & 8.92 & 0 \\ & & & 0 & 0 & 9.02 \end{pmatrix} \times 10^{-12} \quad \mathrm{Pa}^{-1} \tag{A.3}$$

References

[1] T.J. Kazmierski, S. Beeby, Energy harvesting systems. Principles, Modeling and Applications, Springer Science+ Business Media LLC, New York, NY, USA, 2011.

[2] H. Li, C. Tian, Z.D. Deng, Energy harvesting from low-frequency applications using piezoelectric materials, Appl. Phys. Rev. 1 (4) (2014) 041301. Dec 6.

[3] J.M. Ramírez, C.D. Gatti, S.P. Machado, M. Febbo, A multi-modal energy harvesting device for low-frequency vibrations, Extrem. Mech. Lett. 22 (2018) 1–7. Jul 1.

[4] A. Li, K. Goto, Y. Kobayashi, Y. Hara, Y. Jia, Y. Shi, C. Soutis, H. Kurita, F. Narita, K. Otsuka, K. Makihara, Energy harvesting using a magnetostrictive transducer based on switching control, Sens. Actuators A: Phys. 355 (2023) 114303.

[5] M.R. Sarker, S. Julai, M.F. Sabri, S.M. Said, M.M. Islam, M. Tahir, Review of piezoelectric energy harvesting system and application of optimization techniques to enhance the performance of the harvesting system, Sens. Actuators A: Phys. 300 (2019) 111634. Dec 1.

[6] S. Priya, D.J. Inman, Energy Harvesting Technologies, Springer, New York, 2009 (Jan).

[7] B. Berglund, P. Hassmén, R.S. Job, Sources and effects of low-frequency noise, J. Acoust. Soc. Am. 99 (5) (1996) 2985–3002 (May).

[8] Rastegar J., Pereira C., Nguyen H.L. Piezoelectric-based power sources for harvesting energy from platforms with low-frequency vibration. InSmart Structures and Materials 2006: Industrial and Commercial Applications of Smart Structures Technologies 2006 Mar 24 (Vol. 6171, p. 617101). SPIE.

[9] Y. Zhang, T. Wang, A. Zhang, Z. Peng, D. Luo, R. Chen, F. Wang, Electrostatic energy harvesting device with dual resonant structure for wideband random vibration sources at low frequency, Rev. Sci. Instrum. 87 (12) (2016) 125001. Dec 5.

[10] H. Jafari, A. Ghodsi, S. Azizi, M.R. Ghazavi, Energy harvesting based on magnetostriction, for low frequency excitations, Energy 124 (2017) 1–8. Apr 1.

[11] R. Salazar, M. Serrano, A. Abdelkefi, Fatigue in piezoelectric ceramic vibrational energy harvesting: a review, Appl. Energy 270 (2020) 115161. Jul 15.

[12] K. Uchino, Piezoelectric energy harvesting systems—essentials to successful developments, Energy Technol. 6 (5) (2018) 829–848 (May).

[13] S. Suzuki, T. Kawamata, R. Simura, S. Asano, S. Fujieda, R.Y. Umetsu, M. Fujita, M. Imafuku, T. Kumagai, T. Fukuda, Anisotropy of magnetostriction of functional BCC iron-based alloys, Mater. Trans. 60 (11) (2019) 2235–2244. Nov 1.

[14] Y.T. Huang, T. Ono, Magnetostriction of electroplated TbFeCo thin films, J. Magn. Magn. Mater. 577 (2023) 170799. Jul 1.

[15] Y.Y. Liu, J.H. Li, X.L. Li, X. Mu, X.Q. Bao, X.X. Gao, Single Goss grain growth by isothermal annealing in rolled Fe–Al–Ga–NbC sheets, Rare Met. (2018) 1–8. Sep 4.

[16] T. Ben, Y. Kong, L. Chen, F. Chen, X. Zhang, Magnetostriction property modeling of silicon steel considering stress-induced and magnetocrystalline anisotropy, AIP Adv. 13 (2) (2023). Feb 1.

[17] H. Kurita, S.M. binti Fakhruddin, K.Y. Inoue, T. Nakaki, S. Kuroda, Z. Wang, W. Araki, H. Shiku, F. Narita, Energy-harvesting and mass sensor performances of magnetostrictive cobalt ferrite-spattered Fe–Co alloy plate, J. Alloy. Compd. 951 (2023) 169844. Aug 5.

[18] S. Kim, C.J. Thompson, Y. Xin, C. Beekman, Large magnetic anisotropy and magnetostriction in thin films of CoV 2 O 4, Phys. Rev. Mater. 7 (1) (2023) 014408. Jan 20.

[19] Deng Z. Nonlinear modeling and characterization of the Villari effect and model-guided development of magnetostrictive energy harvesters and dampers (Doctoral dissertation, The Ohio State University).

[20] Berbyuk V. Vibration energy harvesting using Galfenol-based transducer. In Active and Passive Smart Structures and Integrated Systems 2013, 2013 Apr 10, (Vol. 8688, pp. 429–440). SPIE.

[21] S. Mohammadi, A. Esfandiari, Magnetostrictive vibration energy harvesting using strain energy method, Energy 81 (2015) 519–525. Mar 1.

[22] M. Ghodsi, H. Ziaiefar, M. Mohammadzaheri, A. Al-Yahmedi, Modeling and characterization of permendur cantilever beam for energy harvesting, Energy 176 (2019) 561–569. Jun 1.

[23] Cullity B.D., Graham C.D. Introduction to magnetic materials. John Wiley & Sons; 2011 Oct 7.

[24] P. Fagan, B. Ducharne, L. Daniel, A. Skarlatos, M. Domenjoud, C. Reboud, Effect of stress on the magnetic Barkhausen noise energy cycles: a route for stress evaluation in ferromagnetic materials, Mater. Sci. Eng.: B 278 (2022) 115650. Apr 1.

[25] O. Hubert, L. Daniel, R. Billardon, Experimental analysis of the magnetoelastic anisotropy of a non-oriented silicon iron alloy, J. Magn. Magn. Mater. 254 (2003) 352–354. Jan 1.

[26] R.C. Hall, Magnetic anisotropy and magnetostriction of ordered and disordered cobalt-iron alloys, J. Appl. Phys. 31 (5) (1960) S157–S158 (May).

[27] S. Somkun, A.J. Moses, P.I. Anderson, P. Klimczyk, Magnetostriction anisotropy and rotational magnetostriction of a nonoriented electrical steel, IEEE Trans. Magn. 46 (2) (2010) 302–305. Jan 19.

[28] C. Mudivarthi, S. Datta, J. Atulasimha, P.G. Evans, M.J. Dapino, A.B. Flatau, Anisotropy of constrained magnetostrictive materials, J. Magn. Magn. Mater. 322 (20) (2010) 3028–3034. Oct 1.

[29] P.G. Evans, M.J. Dapino, Measurement and modeling of magnetic hysteresis under field and stress application in iron–gallium alloys, J. Magn. Magn. Mater. 330 (2013) 37–48. Mar 1.

[30] U. Aydin, P. Rasilo, F. Martin, D. Singh, L. Daniel, A. Belahcen, M. Rekik, O. Hubert, R. Kouhia, A. Arkkio, Magneto-mechanical modeling of electrical steel sheets, J. Magn. Magn. Mater. 439 (2017) 82–90. Oct 1.

[31] B. Ducharne, S. Zurek, L. Daniel, G. Sebald, An anisotropic vector hysteresis model of ferromagnetic behavior under alternating and rotational magnetic field, J. Magn. Magn. Mater. 549 (2022) 169045. May 1.

[32] Li M., Zhang Y., Jing Y., Wang Z., Xie D. Magnetostrictive hysteretic properties estimation of electrical steel sheet under external stress using improved ADSM model. COMPEL-The international journal for computation and mathematics in electrical and electronic engineering. 2022 May 16(ahead-of-print).

[33] A. Sisman, H. Saygin, On the power cycles working with ideal quantum gases: I. The Ericsson cycle, J. Phys. D: Appl. Phys. 32 (6) (1999) 664. Mar 21.

[34] B. Zhang, B. Ducharne, B. Gupta, G. Sebald, D. Guyomar, J. Gao, Experimental sea wave energy extractor based on piezoelectric Ericsson cycles, J. Intell. Mater. Syst. Struct. 29 (6) (2018) 1102–1112 (Apr).

[35] B. Zhang, B. Ducharne, D. Guyomar, G. Sebald, Energy harvesting based on piezoelectric Ericsson cycles in a piezoceramic material, Eur. Phys. J. Spec. Top. 222 (7) (2013) 1733–1743 (Sep).

[36] O. Stupakov, R. Wood, Y. Melikhov, D. Jiles, Measurement of electrical steels with direct field determination, IEEE Trans. Magn. 46 (2) (2010) 298–301. Jan 19.

[37] O. Stupakov, System for controllable magnetic measurement with direct field determination, J. Magn. Magn. Mater. 324 (4) (2012) 631–636. Feb 1.

[38] https://www.jfe-steel.co.jp/en/products/electrical/catalog/f1e-001.pdf

[39] L. Daniel, O. Hubert, N. Buiron, R. Billardon, Reversible magneto-elastic behavior: a multiscale approach, J. Mech. Phys. Solids 56 (3) (2008) 1018–1042. Mar 1.

[40] L. Daniel, M. Rekik, O. Hubert, A multiscale model for magneto-elastic behaviour including hysteresis effects, Arch. Appl. Mech. 84 (9) (2014) 1307–1323 (Oct).

[41] O. Hubert, L. Daniel, Multiscale modeling of the magneto-mechanical behavior of grain-oriented silicon steels, J. Magn. Magn. Mater. 320 (7) (2008) 1412–1422. Apr 1.

[42] N.T. Tung, G. Taxil, H.H. Nguyen, B. Ducharne, M. Lallart, E. Lefeuvre, H. Kuwano, G. Sebald, Ultimate electromechanical energy conversion performance and energy storage capacity of ferroelectric materials under high excitation levels, Appl. Energy 326 (2022) 119984. Nov 15.

[43] G. Sebald, N.T. Tung, G. Taxil, B. Ducharne, J. Chavez, T. Ono, H. Kuwano, E. Lefeuvre, M. Lallart, Piezoelectric small scale generator: towards near-Joule output energy generation, Smart Mater. Struct. (2023). Jun 16.

[44] Z. Deng, M.J. Z, M.J. Dapino, Review of magnetostrictive vibration energy harvesters, Smart Mater. Struct. 26 (10) (2017) 103001. Sep 7.

[45] J. Atulasimha, A.B. Flatau, A review of magnetostrictive iron–gallium alloys, Smart Mater. Struct. 20 (4) (2011) 043001. Mar 8.

[46] Z. Deng, M.J. Dapino, Review of magnetostrictive materials for structural vibration control, Smart Mater. Struct. 27 (11) (2018) 113001. Oct 23.

[47] L. Daniel, B. Ducharne, Y. Liu, G. Sebald, Choosing the best magnetostrictive material for energy harvesting applications: a simple criterion based on Ericsson cycles, J. Magn. Magn. Mater. 587 (2023) 171281. Dec 1.

[48] François D., Pineau A., Zaoui A. Mechanical behaviour of materials. Dordrecht: Kluwer academic publishers; 1998.

Yuanyuan Liu received a graduate degree in electrical engineering from the Institut National des Sciences Appliquées de Lyon (INSA-Lyon), Lyon, France, in 2020. She follows the double degree Ph.D. program between Institut National des Sciences Appliquées de Lyon (France) and Tohoku University (Japan). Her research interests include understanding the multiphysics coupling in materials, magnetostrictive materials, and self-powered energy harvesting.

Laurent Daniel received the Ph.D. degree from the Ecole Normale Supérieure de Cachan, Cachan, France, in 2003, and the Habilitation degree in physics from the Université Paris-

Sud, Orsay, France, in 2011. Since 2015, he has been a Full Professor with the CentraleSupélec, Université Paris-Saclay, Gif sur Yvette, France. His research activities, within the Group of Electrical Engineering of Paris (GeePs), Paris, France, are dedicated to electromechanical and magnetomechanical couplings in materials for electrical engineering applications. He is notably involved in the definition of multiscale methods for the prediction of such coupled phenomena and in the development of dedicated experimental characterization setups. Since 2014, he has been the Director of the Automotive Mechatronics Chair, a partnership between CentraleSupélec, Gif-sur-Yvette; Esigelec, Saint-Etienne du Rouvray, France; and the automotive company Forvia, Nanterre, France.

Gael Sebald received the M.S. degree in electrical engineering and the Ph.D. degree in acoustics from INSA Lyon, Villeurbanne, France, in 2001 and 2004, respectively. He received a Japan Society for Promotion of Science (JSPS) Fellowship for a post-doctoral position in the Institute of Fluid Science, Tohoku University, Sendai, Japan, and worked on piezoelectric materials and their applications. He became an Associate Professor in 2005 and a Professor in 2016 with INSA Lyon. He worked mostly on smart materials (mainly ferroelectrics) and taught general physics. From 2010 to 2011, he was a recipient of the Invited Researcher Fellowship from JSPS to work on piezoelectric energy harvesting at the Department of Nanomechanics, Tohoku University. In 2016, he joined an International Joint Unit (ELyTMaX), founded by CNRS, Université de Lyon, and Tohoku University, working on materials and systems under extreme conditions. He has been in charge of the Research Unit, Tohoku University, since 2017. His research interests include understanding the multiphysics coupling in materials, their application to small power energy harvesting from temperature and vibration, as well as elastocaloric and electrocaloric cooling materials and applications. He also worked on nonlinear dynamics applied to energy harvesting, ferroelectric/ferromagnetic modeling, and fractional calculus applied to hysteresis dynamics and to electromagnetic non-destructive testing.

Mickaël Lallart was born in 1983. He received the graduate degree in electrical engineering and the Ph.D. degree in electronics, electrotechnics, and automatics from the Institut National des Sciences Appliquées de Lyon (INSA-Lyon), Lyon, France, in 2006 and 2008, respectively. He worked with the Laboratoire de Génie Electrique et Ferroélectricité (LGEF). After completing, a post-doctoral fellowship with the Center for Intelligent Material Systems and Structures (CIMSS) in Virginia Tech, Blacksburg, VA, USA, in 2009, he has been hired as an Associate Professor with the Laboratoire de Génie Electrique et Ferroélectricité, and has been appointed as a Full-Time Professor in 2019. Since 2006, he authored or coauthored more than 100 papers in international peer-reviewed journals and authored more than 90 conference papers including 11 personally invited talks and 3 plenary talks. He edited 6 books and participated to 9 book chapters and reviewed more than 250 manuscripts for various journals. Dr. Lallart was the recipient of an invited JSPS research fellowship in Tohoku University, Sendai, Japan, in 2019–2020, and held an invited Adjunct Researcher position in North Western Polytechnical University (NPU), Xi'an, China, in 2018–2020. He was a PI or key partner of National and International Academic Projects funded by French National Research Agency or European Union for instance, and participated to several industrial collaborations as well.

Kanjuro Makihara Doctor of Engineering, received his Bachelor's degree in Aeronautics and Astronautics from the University of Tokyo in 1998 and completed his Ph.D. program from the Graduate School of the University of Tokyo in 2004. Since 2004, he has been an Aerospace Project Research Associate at JAXA/ISAS and has devoted himself to energy recycling vibration suppression for space structures. After serving as a visiting researcher at the University of Cambridge, U.K., he has been working as an Associate Professor of Aerospace Engineering at the Tohoku University since 2011, and in 2019, he became a professor at the Tohoku University. His current research interests involve semiactive vibration suppression, self-powered energy-harvesting, dynamics of flexible structures, and issues pertaining to space debris.

Benjamin Ducharne received the M.S. and Ph.D. degrees in electrical engineering from the University Claude Bernard Lyon I, Villeurbanne, France, in 2001 and 2003, respectively. In 2004, he joined the Institut Montefiore, Liège, Belgium, where he held a post-doctoral position. In 2005, he joined INSA, Lyon, France, as an Associate Professor. From 2018 to 2019, he was a Visiting Scholar and a mid-term Lecturer at Purdue University, West Lafayette, IN, USA. In 2020, he joined ELyTMaX, Tohoku University, Sendai, Japan, as a Full-Time Researcher. His main research interests are magnetic non-destructive testing, ferromagnetic and ferroelectric materials, hysteresis modeling, fractional operators, and multiphysics coupling.